SCIENTIFIC REPORTS

OPEN

SUBJECT AREAS:
BIOINSPIRED MATERIALS
MATERIALS CHEMISTRY

Received
29 May 2014

Accepted
15 August 2014

Published
5 September 2014

Correspondence and requests for materials should be addressed to C.-L.C. (Chunlong.Chen@pnnl.gov)

Tuning calcite morphology and growth acceleration by a rational design of highly stable protein-mimetics

Chun-Long Chen[1,2], Jiahui Qi[1,3], Jinhui Tao[1,2], Ronald N. Zuckermann[1] & James J. DeYoreo[1,2,4]

[1]Molecular Foundry, Lawrence Berkeley National Laboratory, Berkeley, CA 94720, [2]Pacific Northwest National Laboratory, PO Box 999, MS K2-01, Richland, WA 99352, [3]Department of Materials, Imperial College London, London, SW7 2AZ, [4]Department of Materials Science and Engineering, University of Washington, Seattle, WA 98195.

In nature, proteins play a significant role in biomineral formation. One of the ultimate goals of bioinspired materials science is to develop highly stable synthetic molecules that mimic the function of these natural proteins by controlling crystal formation. Here, we demonstrate that both the morphology and the degree of acceleration or inhibition observed during growth of calcite in the presence of peptoids can be rationally tuned by balancing the electrostatic and hydrophobic interactions, with hydrophobic interactions playing the dominant role. While either strong electrostatic or hydrophobic interactions inhibit growth and reduces expression of the {104} faces, correlations between peptoid-crystal binding energies and observed changes in calcite growth indicate moderate electrostatic interactions allow peptoids to weakly adsorb while moderate hydrophobic interactions cause disruption of surface-adsorbed water layers, leading to growth acceleration with retained expression of the {104} faces. This study provides fundamental principles for designing peptoids as crystallization promoters, and offers a straightforward screening method based on macroscopic crystal morphology. Because peptoids are sequence-specific, highly stable, and easily synthesized, peptoid-enhanced crystallization offers a broad range of potential applications.

Biominerals are composed of primarily inorganic minerals and tiny amounts of organic molecules, such as proteins[1]. They perform key functions ranging from mechanical support to self-protection[2–4]. In numerous cases, acidic proteins have been shown to play a critical role in the nucleation, growth and assembly of the mineral components[4–6]. Calcium carbonate ($CaCO_3$) is an abundant and important biomineral in nature, in part because the vast deposits of $CaCO_3$ biominerals produced by marine organisms constitute the largest and most ancient terrestrial reservoir of CO_2[3,7,8]. Proteins commonly presented in natural $CaCO_3$ biominerals are unusually acidic, and many of these acidic proteins, such as Asprich, are amphiphilic[6]. Inspired by protein-directed $CaCO_3$ formation, many efforts have been made to develop synthetic analogs to mimic natural proteins for controlling crystal formation[5,9]. For example, synthetic short-chain peptides promote $CaCO_3$ nucleation and growth in the absence of any biological context[10]. However, application of synthetic protein- and peptide-based materials is problematic, because they exhibit poor stability against thermal and chemical degradation[11,12]. To address this problem, we recently developed a class of non-natural polymers called peptoids that were able to successfully mimic proteins and peptides by providing control over calcite morphology and unprecedented levels of calcite growth rate acceleration at nanomolar concentrations[13].

Peptoids, or poly-N-substituted glycines, were developed to mimic both the structures and functionalities of polypeptides, and bridge the gap between biopolymers and traditional synthetic polymers[14]. In contrast to peptides and proteins, sequence-specific peptoids can be efficiently and cheaply synthesized[15] and exhibit much higher protease stability[12] and structural stability[11,16]. The high degree of control over calcite morphology achieved by peptoids in our previous study indicates they are capable of strongly interacting with calcite surfaces to influence nucleation and growth[13]. In that study, we briefly explored how different peptoid designs, such as the variation of phenethylamine substitution, influence calcite morphology[13]. Measurements of calcite growth rates suggested that only certain peptoids accelerate growth, though exactly which design elements are required was unclear[13]. A systematic investigation of the relationship between peptoid design and control over calcite morphology and growth rate is required to understand the underlying mechanisms of control and to develop general design principles for biomimetic polymers that can act as crystallization promoters for a broad range of industrial applications.

Table 1 | Summary of peptoid designs and corresponding reduction in expression of the {104} faces, acceleration of step speed on the {104} faces, and strength of the hydrophobic and electrostatic interactions as determined by HPLC retention time t (mins) and number of peptoid carboxyl groups (n), respectively. Nce: N-(2-carboxyethyl)glycine, NXpe: N-[2-(X-phenethyl)]glycine, Nab: N-(4-aminobutyl)glycine. v: step velocity with peptoid, v_0: step velocity without peptoid

Peptoids	Different reduction of calcite (104) face formation induced by 51 μM peptoids	Maximum growth acceleration (v/v_0) of two different steps (v_+ and v_-) at lower peptoid concentration	Strength of hydrophobic and electrostatic interactions as determined by HPLC retention time t (mins) and number of peptoid carboxyl groups (n), respectively.
$(Nce)_6(NXpe)_4(Nce)_6$ Pep-**1**: X = 2,4-dichloro; Pep-**2**: X = 4-bormo; Pep-**3**: X = 4-chloro; Pep-**4**: X = 4-hydrogen; Pep-**5**:X = 3,4-dimethoxy	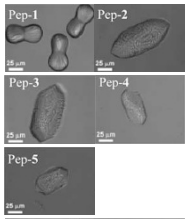	N/A	Pep-**1** (t: 18.7, n: 12); Pep-**2** (t: 17.0, n: 12); Pep-**3** (t: 16.5, n: 12); Pep-**4** (t: 13.9, n: 12); Pep-**5** (t: 11.9, n: 12).
$(NXpe)_4(Nce)_{12}$ Pep-**6**: X = 2,4-dichloro; Pep-**7**: X = 4-bormo; Pep-**8**: X = 4-chloro; Pep-**9**: X = 4-hydrogen; Pep-**10**:X = 3,4-dimethoxy	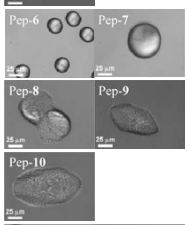	N/A Pep-8: v_+/v_0: 7.0; v_-/v_0: 7.6 (250 nM); Pep-9: v_+/v_0: 29.5; v_-/v_0: 22.4 (1000 nM) N/A	Pep-**6** (t: 19.6, n: 12); Pep-**7** (t: 18.1, n: 12); Pep-**8** (t: 17.4, n: 12); Pep-**9** (t: 14.5, n: 12); Pep-**10** (t: 12.4, n: 12)
$(NXpe)_4(Nab)_4(Nce)_n$ X = 2,4-dichloro Pep-**11**: n = 12; Pep-**12**: n = 8; Pep-**13**: n = 4	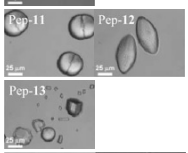	N/A	Pep-**11** (t: 16.9, n: 12); Pep-**12** (t: 17.1, n: 8); Pep-**13** (t: 17.3, n: 4)
$(NXpe)_4(Nce)_8$ Pep-**14**:X = 4-hydrogen; Pep-**15**:X = 4-chloro Pep-**16**: **$(NXpe)_3(Nce)_9$** Pep-**17**: **$(NXpe)_5(Nce)_7$** Pep-**18**: **$(NXpe)_6(Nce)_6$** X = 4-chloro	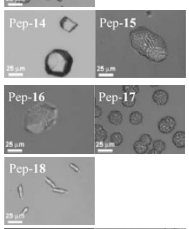	Pep-**14**: v_+/v_0: 22.3; v_-/v_0: 21.5 (50 nM); Pep-**15**: v_+/v_0:10; v_-/v_0: 17 (100 nM) N/A	Pep-**14** (t: 14.7, n: 8); Pep-**15** (t: 17.8, n: 8) Pep-**16** (t: 15.5, n: 9); Pep-**17** (t: 20.4, n: 7); Pep-**18** (t: 22.3, n: 6)
Pep-**19**: **$(NXpe)_2(Nce)_{10}$** Pep-**20**: **$(NXpe)_3(Nce)_9$** Pep-**21**: **$(NXpe)_4(Nce)_8$** Pep-**22**: **$(NXpe)_5(Nce)_7$** X = 2,4-dichloro	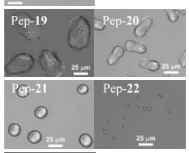	N/A	Pep-**19** (t: N/A, n: 10); Pep-**20** (t: N/A, n: 9); Pep-**21** (t: 20.0, n: 8); Pep-**22** (t: N/A, n: 7).
Pep-**23** (X:2,4-dichloro) **$(Nab)_4(NXpe)_4(Nce)_4$**	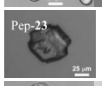	N/A	N/A
Pep-**24** $(NXpe)_4(Nce)_8$ (X: 4-bormo); Pep-**25** $(NXpe)_2(Nce)_{10}$ (X: 4-hydrogen)	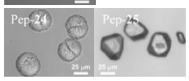	Pep-**24**: v_+/v_0: 3.3; v_-/v_0: 3.9 (500 nM); Pep-**25**: v_+/v_0: 2.5; v_-/v_0: 3.5 (250 nM)	Pep-**24** (t: 18.3, n: 8); Pep-**25** (t: 9.3, n: 10)
$(NXpe)_4(Nce)_8$ Pep-**26** (X:4-Ethyl) Pep-**27** (X:4-Methoxy) Pep-**28**: **$(NceNXpe)_6$** (X: 4-hydrogen)	Pep-**26** N/A 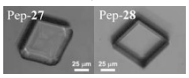	Pep-**26**: v_+/v_0: 2.9; v_-/v_0: 3.9 (1000 nM); Pep-**27**: v_+/v_0: 8.0; v_-/v_0: 24.7 (250 nM); Pep-**28**: v_+/v_0 and v_-/v_0: less than 1.3 (20–800 nM)	Pep-**26** (t: 18.7, n: 8); Pep-**27** (t: 14.1, n: 8); Pep-**28** (t: 16.0, n: 6).

In this article, we report a systematic study of peptoid-induced controls over calcite morphology carried out by rationally tuning the peptoid chemical characteristics, such as the strength and balance of electrostatic and hydrophobic interactions. As summarized in Table 1, the observed dependence of morphology on design shows that the balance between hydrophobic and electrostatic interactions between peptoids and crystal surfaces is important, but hydrophobic interactions play the dominant role. A level of hydrophobicity that leads to moderate peptoid-calcite surface interactions is a critical feature of peptoids that accelerate calcite growth. Moreover, diblock-like peptoids are better candidates for accelerating calcite growth rates than are peptoids in which the hydrophobic and hydrophilic residues are distributed throughout. However, beyond a certain limit, increasing either the electrostatic or hydrophobic interactions reduces the formation of calcite {104} faces to a degree that scales with peptoid concentration. Measurements of peptoid-

calcite binding affinities show that peptoids exhibiting stronger binding to calcite {104} faces and steps were less effective at accelerating calcite growth. Taken together, these observations imply disruption of surface-adsorbed ordered water layers presents the most likely mechanism for peptoid-promoted calcite growth, while strong peptoid-crystal binding is responsible for growth inhibition and morphological control.

Results and discussion

Peptoid design. Extensive experimental and theoretical studies suggest that protein sequence, protein charge and protein hydrophobicity are key features that significantly influence calcite morphology and promotion of growth[3,10,17]. For example, when a protein becomes too hydrophilic, its binding to a crystal surface becomes too strong, and inhibition of crystallization will usually occur rather than promotion of nucleation and growth[18]. Thus the balance between hydrophobic and hydrophilic groups was an important parameter employed in designing peptoids for this research (Table 1). To vary this balance, we designed and synthesized peptoids using the hydrophilic monomer *N*-(2-carboxyethyl) glycine (Nce) to mimic the aspartic or glutamic amino acids, and various substituted *N*-(2-phenylethyl)glycines (NXpe) to mimic hydrophobic amino acids. Because we found previously that the variation of the aromatic substituents caused dramatic differences in calcite morphology[13], in this study, we used a series of substituents to systematically tune peptoid hydrophobicity. We designed and synthesized 28 peptoids (Figure 1, Table 1) by varying: 1) the overall peptoid hydrophobicity through changes in the aromatic substituent (X) and the number of hydrophobic groups (NXpe); 2) the ability to bind to $CaCO_3$ through the number of carboxylic acid groups; 3) the ratio of hydrophobic to hydrophilic groups; and 4) the position of the hydrophobic groups. All of these peptoids were synthesized on an automated robotic synthesizer using solid-phase submonomer cycles as described previously[15].

Controls on calcite morphology. To test if peptoids synthesized in Figure 1 are effective for controlling calcite morphology, we performed $CaCO_3$ mineralization experiments within a sealed desiccator by slow diffusion of CO_2 and ammonia vapor[19] into a solution containing aqueous $CaCl_2$ and peptoids. We found these peptoids were able to dramatically alter calcite morphology, and the effects were highly sequence dependent.

The influence of substituents in the hydrophobic group: hydrophobic interactions. To investigate how different substituents (X) influence growth morphology, 16-mer peptoid analogs Pep-**1** to Pep-**5** (Figure 1a) containing 12 Nce and four NXpe were synthesized. As shown in Figure 2, these five peptoids exhibit different hydrophobicities; Pep-**1** (X = 2,4-dichloro) gives the highest hydrophobicity while Pep-**5** (X = 3,4-dimethoxy) has the lowest hydrophobicity. These peptoids exhibit tunable hydrophobicities in the order Pep-**1** (X = 2,4-dichloro) > Pep-**2** (X = 4-bromo) > Pep-**3** (X = 4-chloro) > Pep-**4** (X = 4-hydrogen) > Pep-**5** (X = 3,4-dimethoxy). Interestingly, although all five are structurally similar, they differed in the degree to which they reduced the formation of the calcite {104} faces. Calcite morphologies obtained in the presence of 51 μM peptoid solutions varied from elongated crystals with multiple facets and pseudo-facets to twisted triangular prisms. Pep-**2**, Pep-**3**, Pep-**4** and Pep-**5** all gave calcite crystals elongated along the [001] direction with three adjacent {104} faces at each terminus of a spindle. A close examination of the elongated crystals indicates that these four peptoids exhibited different influences on the expression of the {104} faces and growth in the [001] direction. Pep-**2** gave the greatest reduction in the formation of the {104} faces, resulting in crystals with the greatest length in the [001] direction. The twisted triangle prism calcite induced by the most hydrophobic peptoid Pep-**1** show almost no {104} faces (Figure 2a), though the morphology still reflected three-fold symmetry along the (001) axis.

When the four NXpe groups were moved to the N-terminal, the resulting peptoid analogs Pep-**6** to Pep-**10** exhibited a similar order of hydrophobicity depending on the choice of substituent X (Figures 3 and S2). These peptoids induced formation of calcite morphologies that varied from elongated crystals to twisted triangle prisms to spherulites (Figure 3). Calcite crystals with spherulitic shapes were induced by peptoids Pep-**6** (X = 2,4-dichloro) and

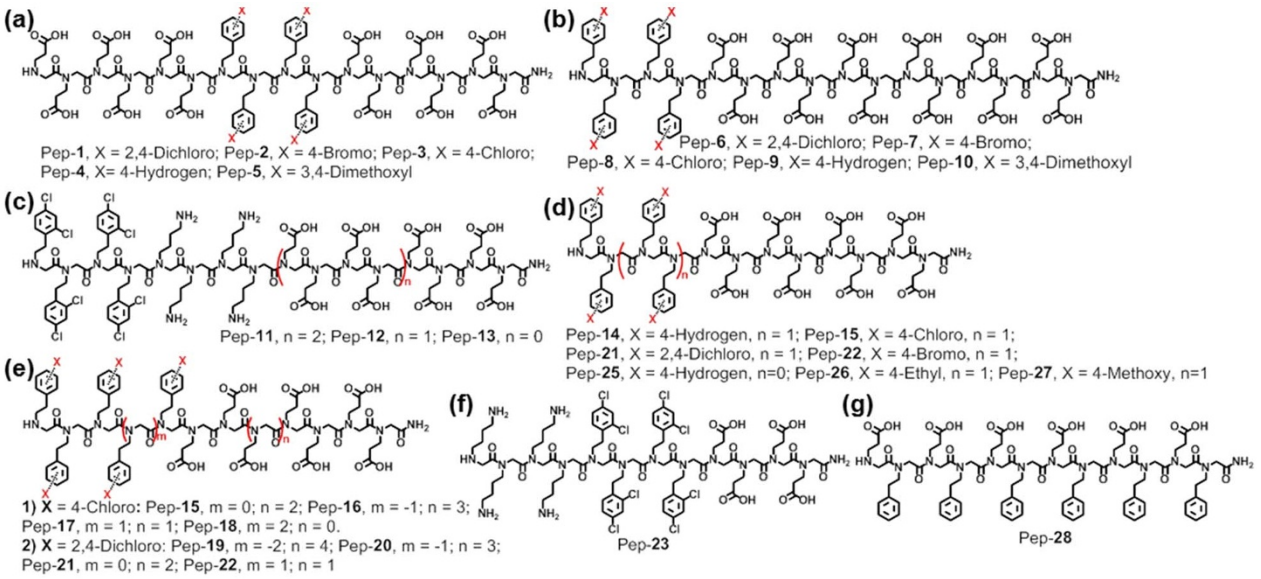

Figure 1 | Structures of 28 peptoids built by varying: 1) the overall peptoid hydrophobicity by (i) varying the aromatic substituent (X) (a, b and d) and (ii) varying the number of hydrophobic groups (d and e), 2) the ability to bind to calcium carbonate through the number of carboxylic acid groups (c, d and e), 3) the ratio of hydrophobic groups to hydrophilic groups (e), and 4) the position of the hydrophobic groups, either as a single block in the N-terminal (b, c and d), in the middle (a and f), or interspersed with the carboxylic acid groups (g).

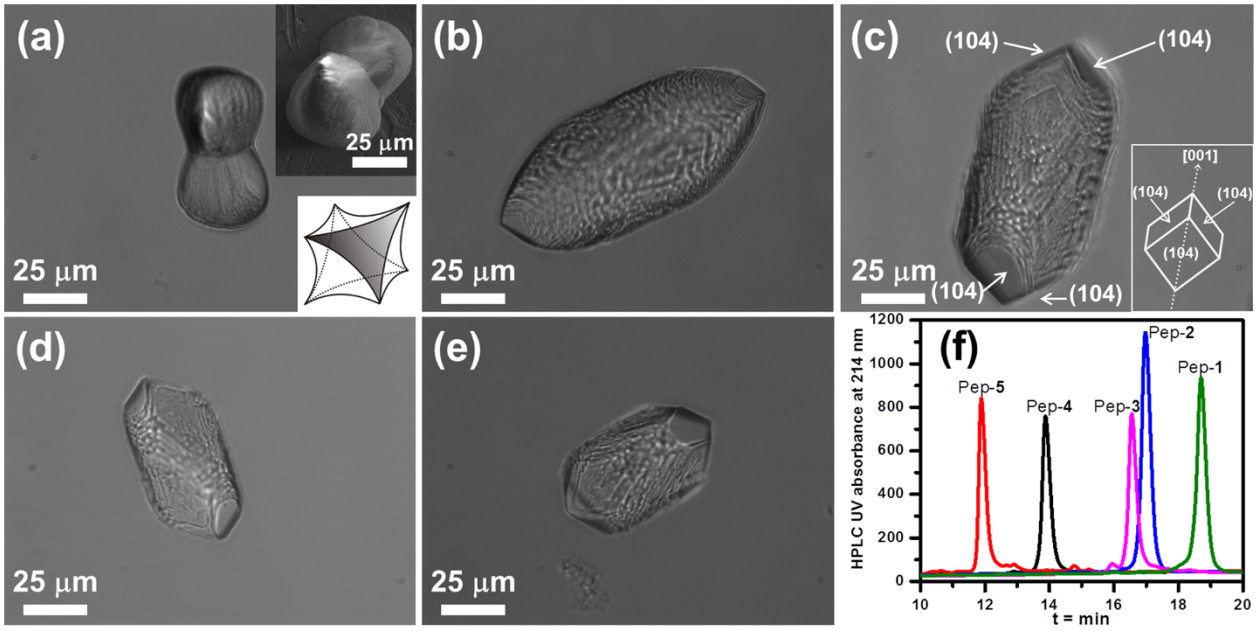

Figure 2 | Calcite crystal morphologies induced by 51 μM peptoids solutions of: (a) Pep-**1** [the inserts are a SEM image and a schematic view of the twisted triangle prism calcite crystal], (b) Pep-**2**, (c) Pep-**3** [the insert is a schematic view of the rhombohedral calcite crystal], (d) Pep-**4** and (e) Pep-**5**. (f) Reverse phase HPLC data shows the relative peptoid hydrophobicities, where longer retention time indicates higher hydrophobicity (5–95% CH_3CN in H_2O at 1 mL/min flow rate; detailed HPLC conditions are provided in the Supporting Information).

Pep-7 (X = 4-bromo), while the less hydrophobic Pep-**9** (X = 4-hydrogen) and Pep-**10** (X = 3,4-dimethoxy) caused the formation of calcite crystals exhibiting elongated morphology with significantly greater expression of the {104} faces. Pep-**8**, which is intermediate in hydrophobicity, produced twisted triangle prisms. All these results show that more hydrophobic peptoids exhibit greater reduction in the formation of the {104} faces. A similar conclusion was reached by comparing morphologies obtained using peptoids with hydrophobic groups in varying positions, either as a single block in the N-terminal or in the middle. As shown in Figures 2c and 3c, because Pep-**8**, with four NClpe groups in the N-terminal, has higher hydrophobicity than does Pep-**3**, with four NClpe groups located in the middle, Pep-**8** induced the formation of twisted triangle prisms exhibiting almost no {104} faces, while crystals grown in the presence of Pep-**3** exhibit significant {104} faces at both ends of the spindle. Similar results were also obtained by using Pep-**2** and Pep-**7** (Figures 2b, 3b and S3).

Although it remains a challenge to determine precisely how peptoids interact with crystal surfaces, these morphological changes clearly show that the degree to which formation of the {104} faces

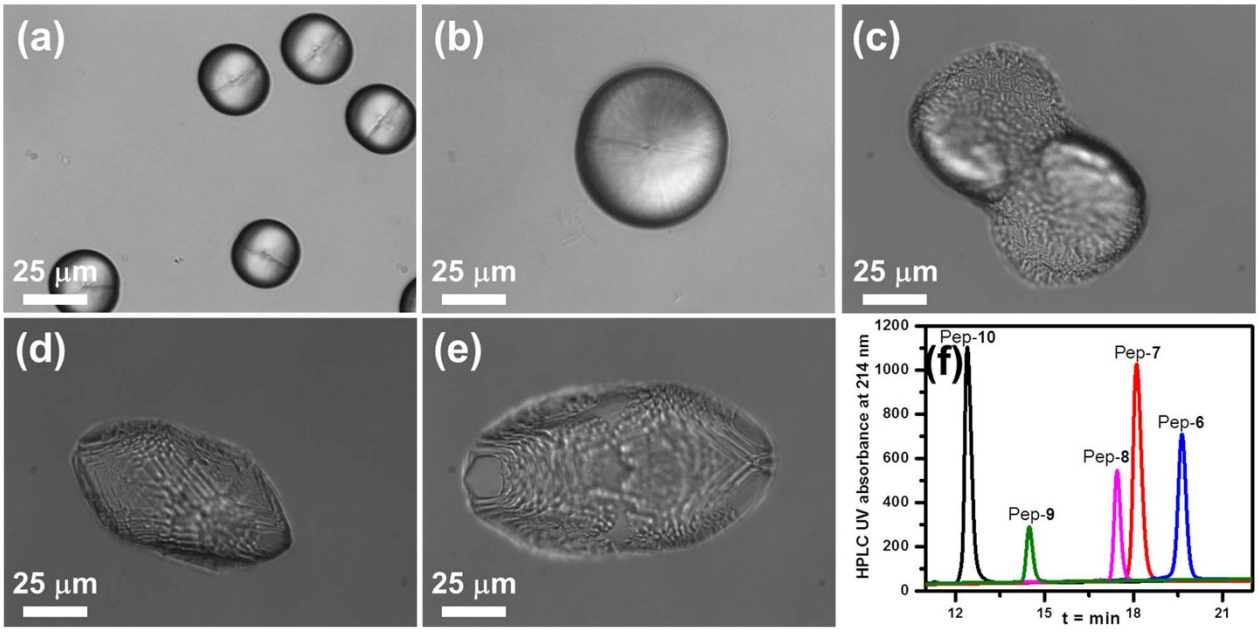

Figure 3 | (a–e) Calcite crystal morphologies induced by 51 μM peptoid solutions of: (a) Pep-**6**, (b) Pep-**7**, (c) Pep-**8**, (d) Pep-**9** and (e) Pep-**10**. (f) Reverse phase HPLC data shows the relative peptoid hydrophobicities, where longer retention time indicates higher hydrophobicity (5–95% CH_3CN in H_2O at 1 mL/min flow rate; detailed HPLC conditions are provided in the Supporting Information).

is reduced increases with greater peptoid hydrophobicity. Because carboxylic acid groups, such as those in propionic acid or acetic acid, have pKas < 5.0[20], and the pH value of the crystallization solutions from the $(NH_4)_2CO_3$ diffusion method is >8.5[21,22], these peptoids predominantly adopt carboxylate form during $CaCO_3$ mineralization, exhibiting both electrostatic and hydrophobic interactions with crystal surfaces. Therefore, structurally similar peptoids having the same number of carboxylic acid groups are expected to exhibit similar electrostatic interactions with crystal surfaces. Thus the differences in the degree to which these peptoids reduce the expression of the {104} faces are due to the variations in hydrophobic interactions. Nonetheless, the level of hydrophobicity alone is not the single determining factor. Although Pep-**1** is slightly more hydrophobic than Pep-7, crystals grown in the presence of Pep-7 exhibits a higher degree of shape modification than does Pep-**1** (Figures 2a, 3b and S3), which shows that monomer sequence, rather than hydrophobicity alone, can also influence the overall reduction in the formation of {104} faces. These results show that varying the substituent (X) in the hydrophobic groups is an effective way to tune peptoid-calcite interactions to achieve morphological control, but these controls can be modulated by the choice of monomer sequence.

The influence of the number of carboxylic acid groups: electrostatic interactions. To investigate the influence of the number of carboxylic acid groups on calcite morphology, calcite growth in the presence of a series of peptoids with varying numbers of carboxylic acid groups was explored. As shown in Figure 4, Pep-**11**, with the largest number of carboxylic acid groups, exhibited the greatest reduction expression of the {104} faces and formed spherulitic crystals. Pep-**13**, which has the smallest number of carboxylic acid groups, produced the largest {104} faces, with the crystals typically exhibiting a truncated rhombohedral morphology (Figure 4c). Pep-**12**, with an intermediate number of carboxylic acid groups, induced formation of spindles exhibiting minor {104} faces (Figures 4 and S4). Because Pep-**11**, Pep-**12** and Pep-**13** have the same hydrophobic domains, they are expected to exhibit similar hydrophobic interactions with the crystal surfaces. This implies the differences in the degree to which formation of the {104} faces is reduced across this series of peptoids are determined by the interactions of the carboxyl groups with the crystals. Because all carboxyl groups of peptoids are deprotonated under $(NH_4)_2CO_3$ diffusion-induced crystallization conditions[21,22], they interact with calcite surface through electrostatic interactions[10,22]. Therefore, we conclude that peptoids with larger numbers of carboxyl groups exhibit greater electrostatic interactions, and the differences in electrostatic interactions cause the different levels of reduction. Similar results were also observed when other peptoids with varying numbers of carboxyl groups were used (Figure S5).

The competition between hydrophobic and electrostatic interactions. From the above discussions, it is clear that both electrostatic and hydrophobic interactions exert important influences on calcite morphology. Peptoids became more effective at reducing {104} face formation when either the number of carboxyl groups was increased or substituents that are more hydrophobic were introduced. To know which of these two interactions plays the predominant role in inhibiting {104} face formation and altering morphology, a small library of 12-mer peptoids with varying ratios of hydrophobic group (n_{NClpe}) to carboxyl group (n_{Nce}) were used (Figures 5 and S6). When $n_{NClpe}/n_{Nce} = 1:3$, the resulting Pep-**16** has the least hydrophobicity (Figure 5f) and the largest number of carboxyl groups. Crystals grown with this peptoid have obvious {104} faces (Figure 5a). In contrast, Pep-**18** ($n_{NClpe}/n_{Nce} = 1:1$), which has the highest hydrophobicity and the smallest number of carboxylic acid groups, induced formation of calcite crystals exhibiting almost no {104} faces (Figure 5d). These results suggest that hydrophobic interactions are more important than electrostatic interactions in reducing the formation of the {104} faces. This trend was also observed when comparing calcite crystal morphologies produced by Pep-**15** ($n_{NClpe}/n_{Nce} = 1:2$) and Pep-**17** ($n_{NClpe}/n_{Nce} = 5:7$) (Figures 5b and 5c). To further test this conclusion, we designed another library of 12-mer peptoids by using N-2-[(2,4-dichlorophenyl) ethyl]glycine (N2Clpe) as the hydrophobic monomers and Nce as the hydrophilic monomers and varying the ratio of hydrophobic groups (n_{N2Clpe}) to carboxylic acid groups (n_{Nce}) (Figure 6). As expected, Pep-**19** with the smallest ratio ($n_{N2Clpe}/n_{Nce} = 1:5$) induced the formation

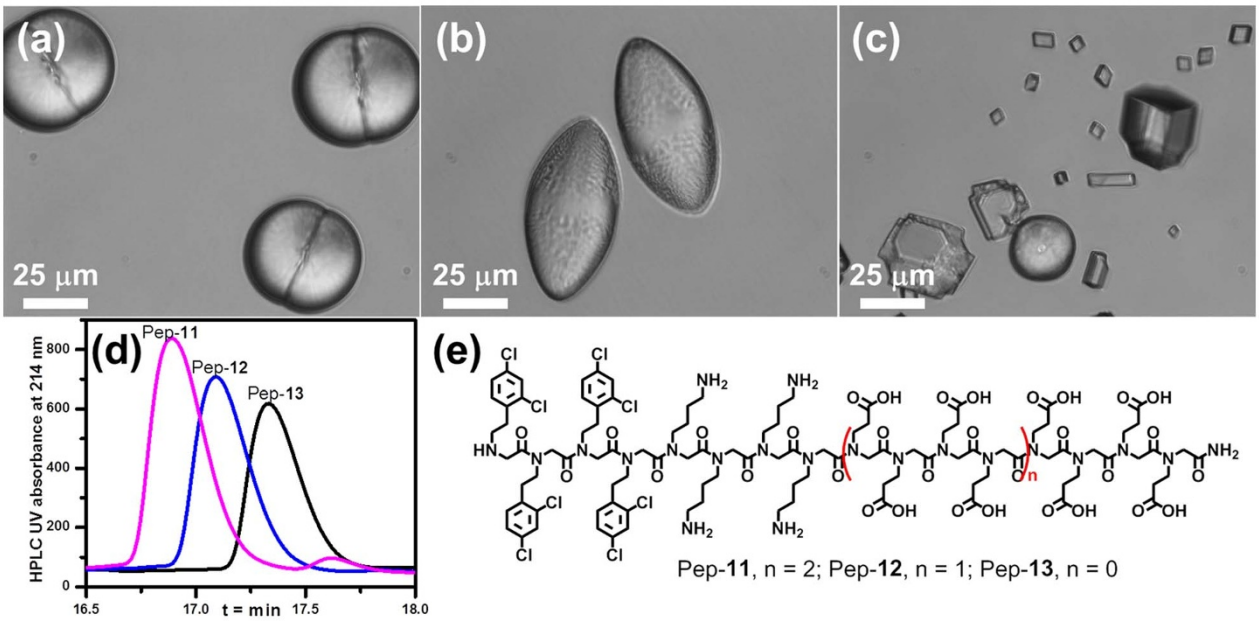

Figure 4 | (a–c) Calcite crystal morphologies induced by 51 μM peptoid solutions of: (a) Pep-**11**, (b) Pep-**12** and (c) Pep-**13**. Peptoids with a larger number of carboxyl groups exhibit stronger reduction in the expression of the {104} faces. (d) Reverse phase HPLC data shows the relative hydrophobicities, where longer retention time indicates higher hydrophobicity (5–95% CH_3CN in H_2O at 1 mL/min flow rate; detailed HPLC conditions are provided in the Supporting Information). (e) Structures of peptoids Pep-**11**, Pep-**12** and Pep-**13**.

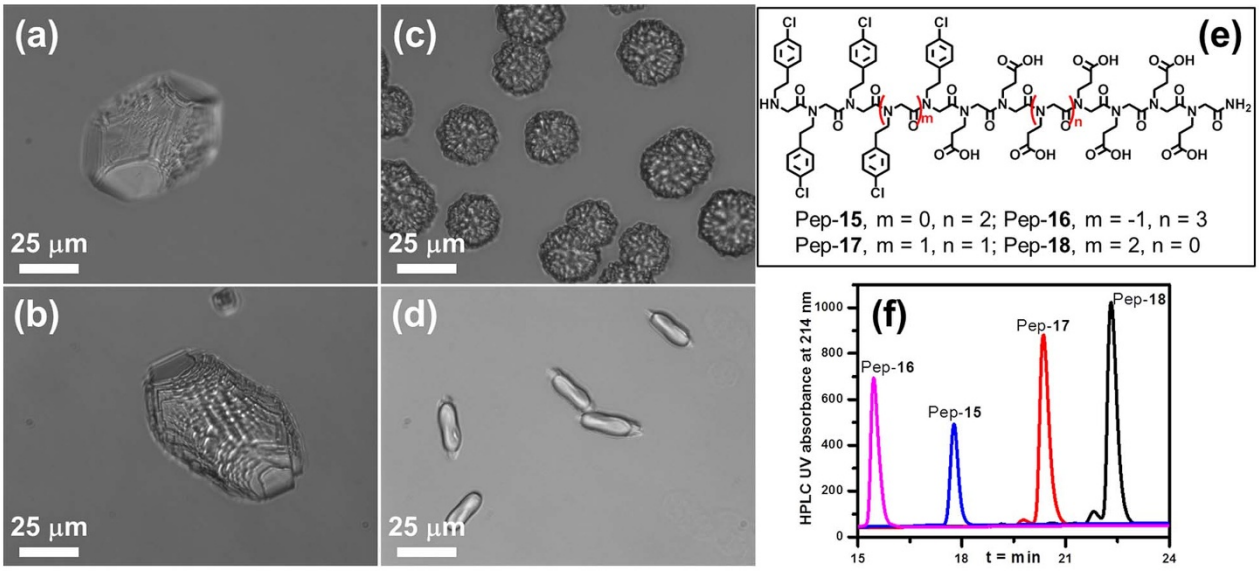

Figure 5 | (a–d) Calcite morphologies induced by 51 μM peptoid solutions: (a) Pep-**16**, (b) Pep-**15**, (c) Pep-**17** and (d) Pep-**18**. (e) Structures of peptoids Pep-**15**, Pep-**16**, Pep-**17** and Pep-**18**. (f) Reverse phase HPLC data shows the relative peptoid hydrophobicities, where longer retention time indicates higher hydrophobicity (5–95% CH_3CN in H_2O at 1 mL/min flow rate; detailed HPLC conditions are provided in the Supporting Information).

of calcite crystals with the largest {104} faces (Figure 6a), confirming that the hydrophobic interaction dominates the electrostatic interaction in reducing formation of the {104} faces.

The influence of peptoid concentration. Previous studies by us as well as others showed that additive-surface interactions are highly concentration dependent[10,13,23]. To test the hypothesis that peptoid concentration significantly influences expression of the {104} faces, we varied the concentrations of selected peptoids. As shown in Figure 7a, 51 μM solutions of Pep-**23** induced formation of calcite crystals exhibiting a unique morphology with truncated corners and edges of regular rhombohedra. These truncated faces can be assigned to (110) and (01l) faces; calcite crystals with similar faces have been obtained using peptides[24] and natural proteins[25]. When the Pep-**23** concentration was increased to 146 μM, the fractional area of the {104} faces was significantly decreased (Figure 7b), resulting in a spicule-like morphology with increased truncation of the crystal faces. Higher concentration Pep-**23** solutions exhibited much greater reduction in the formation of the {104} faces than did lower concentration solutions. This concentration-dependent effect became much more obvious when these peptoid-modified crystals were overgrown for another two days (Figure 7). Significant expression of the {104} faces was still observed in the overgrown calcite crystals when 51 μM solutions of Pep-**23** were used (Figure 7c), while the overgrown calcite crystals produced with 146 μM solutions of Pep-**23** exhibited almost no {104} crystal faces and formed a spicule-like morphology with sharp edges (Figure 7d). Because the faces expressed by a crystal reflect the slowest growth

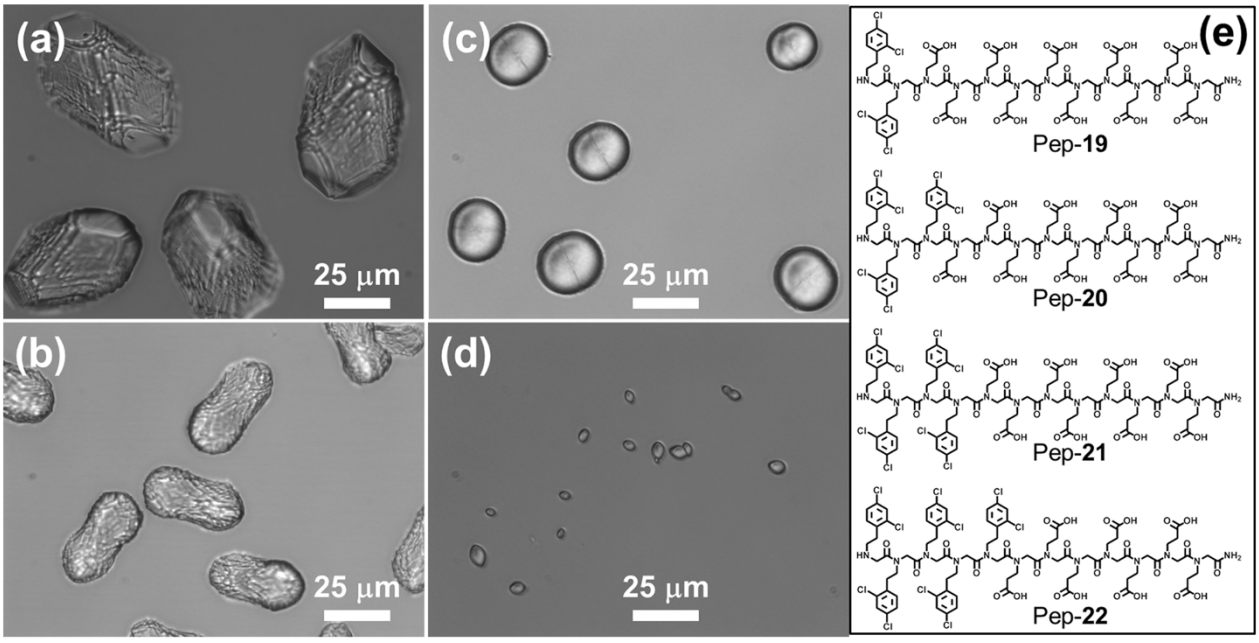

Figure 6 | (a–d) Calcite morphologies induced by 51 μM peptoid solutions of: (a) Pep-**19**, (b) Pep-**20**, (c) Pep-**21** and (d) Pep-**22**. (e) Structures of peptoids Pep-**19**, Pep-**20**, Pep-**21** and Pep-**22**.

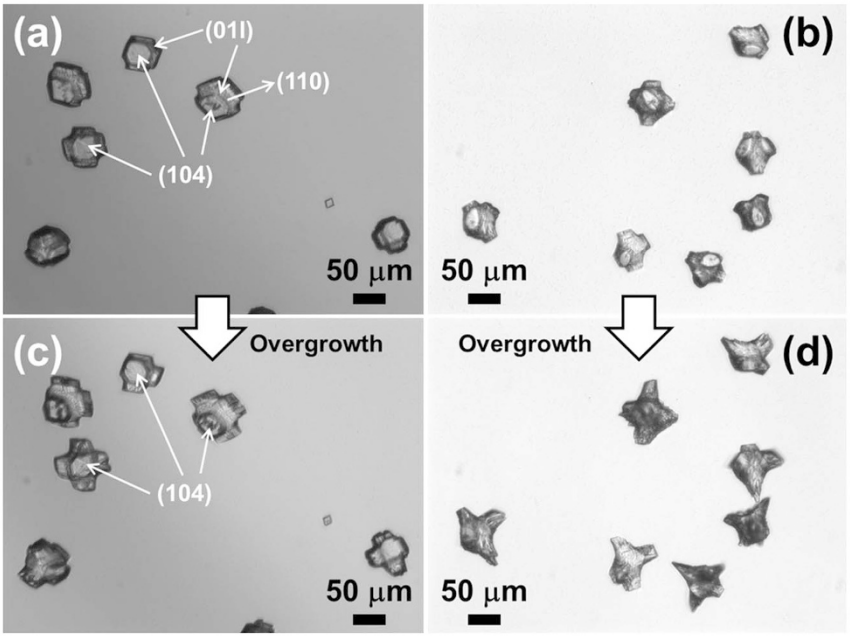

Figure 7 | (a–d) Morphology of calcite crystals grown in the presence of peptoid solutions of: (a) 51 μM Pep-**23**, (b) 146 μM Pep-**23**, (c, d) Overgrown calcite crystals induced by (c) 51 μM solutions of Pep-**23** and (d) 146 μM solutions of Pep-**23**. Some calcite {104}, (110) and (01l) faces are labeled in white.

directions, reduced expression of the {104} faces can be interpreted in terms of selective peptoid adsorption that favors the expression of new faces. When peptoid concentration is increased, peptoids exhibits a higher adsorption, thus inducing greater inhibition in the expression of the {104} faces. This same concentration-dependent behavior was also observed with other peptoids (Figure S7).

Peptoid competition assays for further investigations of hydrophobic and electrostatic interactions. To further understand peptoid-controlled calcite morphology and explain the interactions between peptoids and crystal surface, the effects of combining two different peptoids with 1 : 1 molar ratios were observed. As shown in Figure 8a, twisted triangle prisms were formed when a mixture of 51 μM Pep-**8** and 51 μM Pep-**15** was used. These crystals exhibited almost the same morphologies as those grown in the presence of Pep-**8** alone (Figures 3C, S2c, S3e, S5c, and S7d). Both Pep-**8** and Pep-**15** contain the same monomers, NClpe and Nce; the only difference is that Pep-**8** has four additional Nce groups. Therefore, these results are consistent with our conclusion that, when the hydrophobic block is unchanged, the magnitude of the electrostatic interaction, as controlled by number of carboxyl groups, determines the influence on crystal morphology.

When a mixture of a 51 μM solution of Pep-**15** and a 51 μM solution of Pep-**21** was used, the calcite crystals exhibited spherulitic shapes (Figure 8b), similar to those formed in presence of only

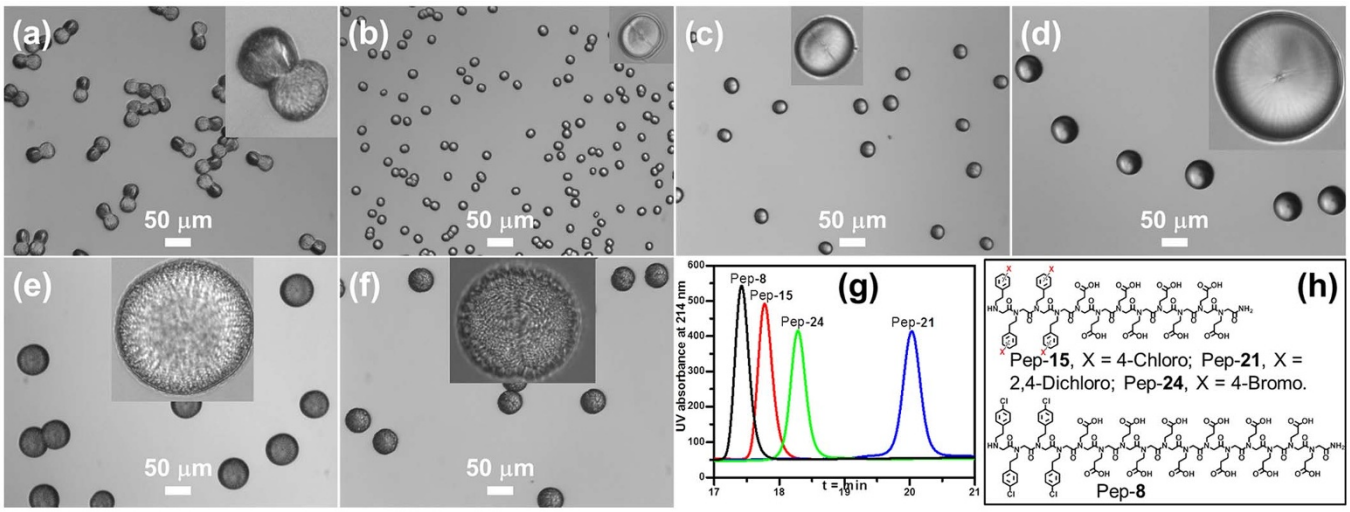

Figure 8 | (a–f) Calcite morphologies obtained in the presence of peptoids or peptoid mixtures: (a) a mixture of 51 μM Pep-**8** and 51 μM Pep-**15**, (b) a mixture of 51 μM Pep-**15** and 51 μM Pep-**21**, (c) only 51 μM Pep-**21**, (d) a mixture of 51 μM Pep-**8** and 51 μM Pep-**21**, (e) a mixture of 51 μM Pep-**8** and 51 μM Pep-**24** and (f) only 51 μM Pep-**24**. Inserts are magnified calcite crystals. (g) Reverse phase HPLC data to show the relative peptoid hydrophobicities, where longer retention time indicates higher hydrophobicity (5–95% CH_3CN in H_2O at 1 mL/min flow rate; detailed HPLC conditions are provided in the Supporting Information). (h) Structures of peptoids Pep-**8**, Pep-**15**, Pep-**21** and Pep-**24**.

51 μM solutions of Pep-**21** alone (Figure 8c). Both Pep-**15** and Pep-**21** contain eight Nce and four NXpe groups; the only difference is in the identity of the substituent X, which renders Pep-**21** more hydrophobic than Pep-**15** (Figure 8g). Therefore, these results are consistent with our conclusion that for the same number of carboxyl groups, the degree of hydrophobicity largely determines calcite morphology. Similar results were obtained when mixtures of either Pep-**8** and Pep-**21** or Pep-**8** and Pep-**24** were used (Figure 8).

Peptoid-promoted calcite growth. To determine whether the extent to which a peptoid reduces {104} face formation at 51 μM peptoid concentration can be used as a straightforward method for screening peptoids to identify those that accelerate {104} face step growth at lower peptoid concentration, in situ atomic force microscopy (AFM) was used to measure step speeds on {104} faces as a function of peptoid concentration.

The influence of hydrophobic and electrostatic interactions on promoting calcite growth rate. Calcite {104} step speeds without (v_0) and with (v) peptoids at different peptoid concentrations were measured at a $CaCO_3$ supersaturation of 0.14 (supersaturation is defined in the Supporting Information). As shown in Figure 9, Pep-**14** enhanced calcite growth rates by ~23-fold at 50-nM levels, while achieving maximum growth acceleration with Pep-**9** required ~1000 nM. Pep-**9** and Pep-**14** both have four hydrophobic groups (Npe) in the N-terminal, but they have different numbers of carboxylic acid groups (Nce). Because Pep-**9** has four more Nce groups than does Pep-**14**, Pep-**9** exhibits greater electrostatic interactions with the crystal. Similar results were observed for solutions containing Pep-**15** and Pep-**8**, respectively (Figure S8). Pep-**8**, which has four additional carboxylic acidic groups, was much less effective than Pep-**15** for achieving acceleration and the peptoid concentration at maximum acceleration shifted from ~100 nM for Pep-**15** to ~250 nM for Pep-**8**. These results indicate that peptoids become less effective in accelerating calcite {104} step growth if the electrostatic interactions become too strong.

To investigate how different substituents (X) in hydrophobic groups influence growth acceleration, a series of 12-mer peptoids with similar diblock-like structures but varied hydrophobicities were used (Figure 10). Pep-**15** (X = 4-chloro) gave maximum accelerations of ~10-fold and 17-fold at 100 nM, while Pep-**24** (X = 4-bromo) achieved only ~3.3-fold and 3.9-fold accelerations at a concentration of 500 nM. Pep-**14**, Pep-**15** and Pep-**24** all have eight Nce groups, but have different substituents (X) in the four hydrophobic groups (NXpe). Pep-**24** is the most hydrophobic, while Pep-**14** (X = 4-hydrogen) is the least. These results indicate that, as with the electrostatic interactions, peptoids become less effective at accelerating calcite {104} step growth if the hydrophobic interactions become too strong.

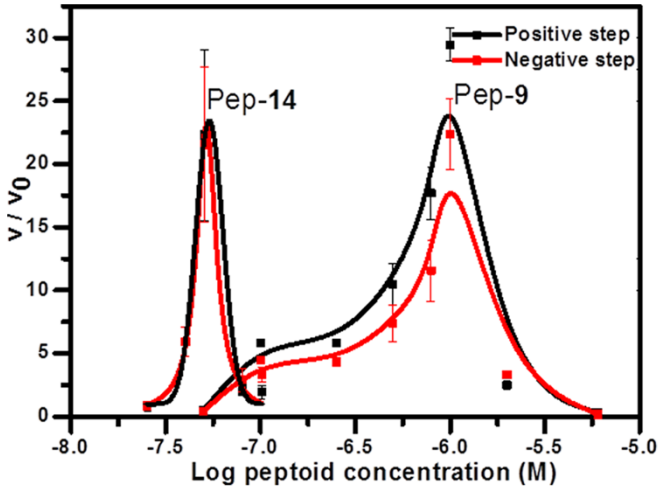

Figure 9 | Measured enhancement of calcite {104} step speeds as a function of log Pep-9 or Pep-14 concentration as determined by in situ AFM. Normalized propagation rates are shown as the ratio of step velocities in the presence (v) and absence (v_0) of peptoids.

The importance of hydrophobicity in designing peptoids as promoters was further demonstrated by using Pep-**25** and Pep-**26** as a hydrophilic control and a hydrophobic control, respectively. As shown in Figure 10b, when peptoids are located in the correct hydrophobic region, such as Pep-**27** and Pep-**14**, they are better candidates as accelerators that efficiently promote calcite crystal growth. The more hydrophilic Pep-**25** and the more hydrophobic Pep-**26** both exhibit much less effectiveness at accelerating step speeds (Figure 10). These results further prove that a correct balance of hydrophobicity and hydrophilicity, giving a moderate peptoid-calcite surface interaction, is a critical feature of peptoids that serve as accelerators of calcite crystal growth.

Interestingly, when two peptoid monomers were changed from diblock-like structures to an alternating pattern, the resulting peptoids exhibited a dramatic difference in enhancement of calcite {104} step growth. Although Pep-**28** (Figure 1g) has the same number of each of two monomers as Pep-**14**, Pep-**28** exhibits a moderate hydrophobicity slightly higher than Pep-**14** but lower than Pep-**15**, Pep-**28** showed almost no acceleration[13] (Figure 10).

Because both hydrophobic and electrostatic interactions exert important influences on both morphology and {104} growth rate, we reasoned that observing the extent to which a peptoid alters the morphology by reducing the formation of the calcite {104} faces might provide a simple means for screening peptoids as growth promoters. Indeed, although 51 μM solutions of Pep-**14**, Pep-**15** and Pep-**24** all reduced the formation of these faces, Pep-**24**, the least effective peptoid at accelerating step speeds, exhibited the greatest reduction in formation of the {104} faces (Figures 8f and S9). Similar correlations were found by comparing calcite morphologic and kinetic controls produced by peptoids Pep-**9** and Pep-**14**, or Pep-**8** and Pep-**15** (Figures 3, 9, S5, S8, and S9). These results indicate that though the ability to reduce formation of the {104} faces is an important feature of peptoids that promote calcite growth, peptoids like Pep-**14** exhibiting a moderate degree of reduction at 51 μM are better candidates for promoters of calcite growth at lower concentration.

Peptoid-calcite binding affinities. To better understand peptoid-induced acceleration, Pep-**14** and Pep-**28**[13] were used for quantifying peptoid-calcite binding. AFM-based dynamic force spectroscopy provides a quantitative probe of interactions between a single molecule and mineral surfaces by measuring the forces it takes to rupture the molecules-surface bond[26]. To this end, we functionalized the tips of AFM cantilevers with either Pep-**14** or Pep-**28** using a similar method described previously[27]. The modified AFM probe tips were then brought in contact with a calcite {104} surface in a solution at equilibrium with calcite. A set of force-distance curves was acquired for each peptoid at retraction velocities in the range of 200–10000 nm/s. The mean rupture forces were then plotted versus the loading (i.e., tip retraction) rate (Figure 11).

The fit of these data (Figure 11a) using the multi-bond model[28] gave a single-molecule binding free energy for Pep-**28** of $\Delta G_{ba} = -4.60 \pm 0.07\ K_BT$. Similarly, fitting data of Pep-**14** (Figure 11b) yields a single-molecule binding free energy of $\Delta G_{ba} = -2.81 \pm 0.21\ K_BT$. These results demonstrate that Pep-**28** exhibits stronger binding to the {104} surface than does Pep-**14**. Given the similarity in structure and size, these differences should correspond to relative lifetimes of adsorption of $\exp(4.6-2.8) = 6.0$. At low concentrations, where coverage is proportional to concentration, this difference also corresponds to a Pep-28 coverage that is greater than that of Pep-14 by the same factor. We further performed AFM-based friction force

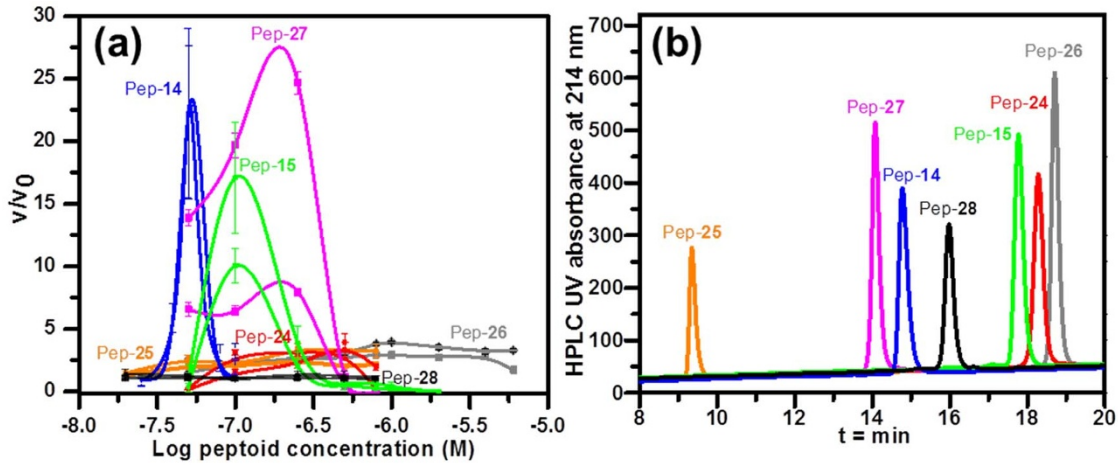

Figure 10 | (a) Measured enhancement of calcite {104} step speeds as a function of log peptoid concentration. Normalized propagation rates are shown as the ratio of step velocities in the presence (v) and absence (v_0) of peptoids. (b) Reverse phase HPLC data to show the relative peptoid hydrophobicities, where longer retention time indicates higher hydrophobicity. Peptoids that efficiently promote calcite crystal growth have retention times of 14–15 min (47%–50% CH_3CN in H_2O at 1.0 mL/min flow rate).

studies using similarly peptoid-modified AFM probes. The average friction force for Pep-**28** interacting with {104} steps was 31.4 pN, while Pep-**14** functionalized AFM tip exhibited a 16.7 pN friction force while interacting with {104} steps (Figure S7), again suggesting a relative lifetime and coverage that favors Pep-**28** binding to the steps. These results indicate that Pep-**28** exhibits stronger binding affinity, longer adsorption lifetime, and greater coverage than Pep-**14** does to both the {104} face and steps.

Proposed mechanism of peptoid-promoted calcite growth: Disruption of the surface-adsorbed water layers. Our results show that a moderate degree of peptoid-surface interaction is a critical feature of peptoids that promote calcite growth. However, when peptoid-surface interactions become too strong, peptoids are less effective promoters. A number of simulations predict that displacing surface-adsorbed ordered water layers from calcite surfaces is the most energetically costly step in the addition of solute ions to the crystal[29,30]. Other simulations show that electrostatic interactions between carboxylate groups of acidic peptides and Ca^{2+} ions in the calcite lattice lead to strong binding affinity to calcite surfaces and steps, providing an explanation for the reported inhibition of calcite growth by such peptides[31,32]. When combined with the observations reported above, these predictions suggest a mechanistic picture of peptoid-induced morphological control and growth acceleration.

First, the morphological, kinetic, and force spectroscopy results presented above indicate that the carboxylate groups on peptoids behave like those on acidic peptides; they bind the peptoids to the crystal surface and steps. Second, moderate hydrophobicity, when created through a di-block arrangement, leads to significant growth acceleration. Thus, as illustrated in Figure 12, we hypothesize that the polar groups serve as the "glue" to bring the hydrophobic groups to the proximity of the surface, where they act to disrupt the adsorbed water layer. The di-block structure is critical, because it allows the carboxylate groups to bind while leaving the hydrophobic block free to disrupt the water layer. Moreover, taking the case of Pep-**14** and Pep-**28** as specific examples, we suggest that the moderate binding free energy (-2.8 K_BT) between Pep-**14** and the {104} face suggests that Pep-**14** reversibly interacts with the calcite surface on a time scale that is rapid enough to allow solute ions to freely attach, but still maintains sufficient coverage to disrupt the water layer and effectively accelerate calcite step growth. In contrast, the stronger binding energy of Pep-**28** (-4.6 K_BT) combined with its alternating Npe-Nce structure implies that the rate of unbinding is much less

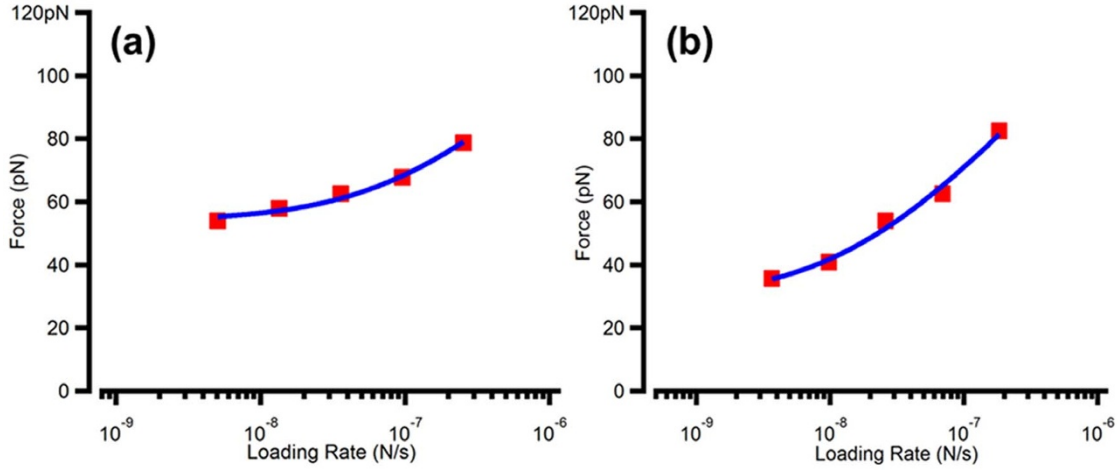

Figure 11 | **The mean rupture force between peptoids and calcite {104} faces at different loading rates.** Fitting these data yields a single-molecule binding free energy. (a) Pep-**28** and (b) Pep-**14**.

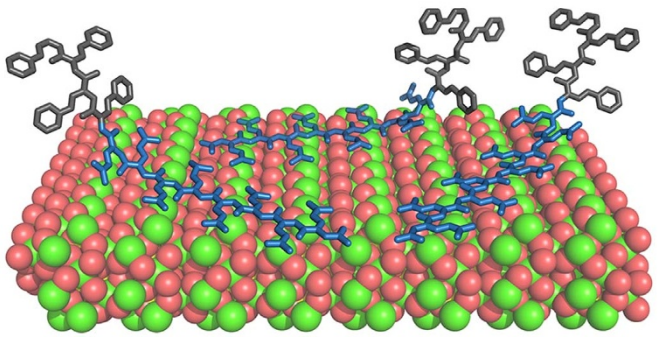

Figure 12 | A proposed model to show how diblock-like peptoids Pep-14 bind to calcite {104} face for disrupting the surface adsorbed water layers for step growth accelerations. Diblock-like peptoids are shown in stick model with hydrophilic Nce groups in blue and hydrophobic Npe groups in gray.

and the hydrophobic groups are held close to the surface, reducing their ability to disrupt the adsorbed water layer and interfering with solute attachment.

For diblock-like peptoids $[(NXpe)_4(Nce)_n]$, a change of the number of carboxyl groups (n) or the substituent (X) in hydrophobic groups is expected to cause changes in both peptoid-surface interactions and levels of water-layer disruption. For example, by increasing the number of carboxylic acid groups from eight to twelve, Pep-**9** exhibits greater electrostatic interactions with calcite surface than does Pep-**14**, resulting in stronger binding to {104} faces and steps. Thus Pep-**9** exhibits a longer adsorption lifetime and greater coverage than does Pep-**14** on both the {104} faces and steps; the rate of unbinding is much less and the hydrophobic groups $(Npe)_4$ are closer to the surface. Thus Pep-**9** is less effective at disrupting of the adsorbed water layer and more likely to interfere with solute attachment, leading to poor performance in promoting growth (Figure 9).

Finally, when the hydrophobicity of a diblock-like peptoid becomes too large due to a change in speciation or increase in the number of the substituents (X), the hydrophobic repulsion with the water is expected to become so great that the hydrophobic block is driven to adsorb to the crystal surface, increasing the peptoid-calcite dissociation constant (K_d) due to the hydrophobic effect[33]. This reduces its ability to disrupt the adsorbed water layer and increases the likelihood it interferes with solute attachment.

Conclusions

In summary, we have shown that a rational design of peptoids with controllable balance of electrostatic and hydrophobic interactions enabled us to tune both the morphology and growth rate of calcite (Table 1). We found that peptoids became more effective at reducing expression of the {104} faces when a) the number of carboxyl groups was increased, b) peptoid hydrophobicity was increased by introducing more hydrophobic substituents or c) peptoid concentration was increased. Moreover, while the balance between hydrophobic and electrostatic interactions was important, hydrophobicity played the dominant role. Studies of peptoid-modified calcite {104} step speeds showed that the degree to which peptoids reduce formation of the {104} faces at higher peptoid concentration can be used as a straightforward method to screen for peptoids that promote growth at lower peptoid concentration. A level of hydrophobicity that leads to moderate peptoid-calcite surface interactions is a critical feature of peptoids that accelerate calcite growth. The results imply disruption of surface-adsorbed ordered water layers presents the most likely mechanism of peptoid-promoted calcite growth.

Given that peptoids are sequence-specific and highly stable, and subtle changes in the electrostatic-hydrophobic balance or the pattern of peptoid monomers results in a dramatic changes in calcite morphology and growth rate acceleration, we conclude that rational design of peptoids offers a viable approach to mimicking natural proteins that control crystal nucleation and growth. Because the number of primary amines available for building peptoid side chains far exceeds the number of natural amino acids, the "toolkit" for designing peptoids that are effective at controlling crystallization is expected to be broader than that available through synthetic proteins. Moreover, because all biominerals and many important synthetic crystals are grown from aqueous solutions, peptoids may also provide highly stable promoters of crystallization for a broad range of biomedical and industrial applications.

Full methods and any associated characterization methods are available in the Supplementary Information.

1. Mann, S. *et al.* Crystallization at inorganic-organic interfaces - biomimerals and biomimetic synthesis. *Science* **261**, 1286–1292, doi:10.1126/science.261.5126.1286 (1993).
2. Chen, C. L. & Rosi, N. L. Peptide-based methods for the preparation of nanostructured inorganic materials. *Angew. Chem., Int. Ed.* **49**, 1924–1942, doi:10.1002/anie.200903572 (2010).
3. Evans, J. S. "Tuning in" to mollusk shell nacre- and prismatic-associated protein terminal sequences. Implications for biomineralization and the construction of high performance inorganic-organic composites. *Chem. Rev.* **108**, 4455–4462, doi:10.1021/cr078251e (2008).
4. Margolis, H. C., Beniash, E. & Fowler, C. E. Role of macromolecular assembly of enamel matrix proteins in enamel formation. *J. Dent. Res.* **85**, 775–793 (2006).
5. Meldrum, F. C. & Coelfen, H. Controlling mineral morphologies and structures in biological and synthetic systems. *Chem. Rev.* **108**, 4332–4432, doi:10.1021/cr8002856 (2008).
6. Gotliv, B. A. *et al.* Asprich: A novel aspartic acid-rich protein family from the prismatic shell matrix of the bivalve Atrina rigida. *ChemBioChem* **6**, 304–314, doi:10.1002/cbic.200400221 (2005).
7. Meldrum, F. C. Calcium carbonate in biomineralisation and biomimetic chemistry. *Int. Mater. Rev.* **48**, 187–224, doi:10.1179/095066003225005836 (2003).
8. Stanley, S. M. Effects of global seawater chemistry on biomineralization: Past, present, and future. *Chem. Rev.* **108**, 4483–4498, doi:10.1021/cr800233u (2008).
9. Sommerdijk, N. & de With, G. Biomimetic $CaCO_3$ mineralization using designer molecules and interfaces. *Chem. Rev.* **108**, 4499–4550, doi:10.1021/cr078259o (2008).
10. Elhadj, S., De Yoreo, J. J., Hoyer, J. R. & Dove, P. M. Role of molecular charge and hydrophilicity in regulating the kinetics of crystal growth. *Proc. Natl. Acad. Sci. U. S. A.* **103**, 19237–19242, doi:10.1073/pnas.0605748103 (2006).
11. Sanborn, T. J., Wu, C. W., Zuckerman, R. N. & Barron, A. E. Extreme stability of helices formed by water-soluble poly-N-substituted glycines (polypeptoids) with alpha-chiral side chains. *Biopolymers* **63**, 12–20, doi:10.1002/bip.1058 (2002).
12. Miller, S. M. *et al.* Comparision of the proteolytic susceptibilities of homologous L-amino-acid, and N-substituted glycine peptide and peptoid oligomers. *Drug Dev. Res.* **35**, 20–32 (1995).
13. Chen, C. L., Qi, J. H., Zuckermann, R. N. & DeYoreo, J. J. Engineered biomimetic polymers as tunable agents for controlling $CaCO_3$ mineralization. *J. Am. Chem. Soc.* **133**, 5214–5217, doi:10.1021/ja200595f (2011).
14. Sun, J. & Zuckermann, R. N. Peptoid Polymers: A highly designable bioinspired material. *ACS Nano* **7**, 4715–4732, doi:10.1021/nn4015714 (2013).
15. Zuckermann, R. N., Kerr, J. M., Kent, S. B. H. & Moos, W. H. Efficient method for the preparation of peptoids oligo(N-substituted glycines) by submonomer solid-phase synthesis. *J. Am. Chem. Soc.* **114**, 10646–10647, doi:10.1021/ja00052a076 (1992).
16. Rosales, A. M., Murnen, H. K., Zuckermann, R. N. & Segalman, R. A. Control of crystallization and melting behavior in sequence specific polypeptoids. *Macromolecules* **43**, 5627–5636, doi:10.1021/ma1002563 (2010).
17. Freeman, C. L., Harding, J. H., Quigley, D. & Rodger, P. M. Structural control of crystal nuclei by an eggshell protein. *Angew. Chem., Int. Ed.* **49**, 5135–5137, doi:10.1002/anie.201000679 (2010).
18. Jones, F. & Ogden, M. I. Controlling crystal growth with modifiers. *CrystEngComm* **12**, 1016–1023, doi:10.1039/b918849e (2010).
19. Addadi, L. & Weiner, S. Interactions between acid proteins and crystals - stereochemical requirements in biomineralization. *Proc. Natl. Acad. Sci. U. S. A.* **82**, 4110–4114, doi:10.1073/pnas.82.12.4110 (1985).
20. Dippy, J. F. J. The dissociation constants of monocarboxylic acids; Their measurement and their significance in theoretical organic chemistry. *Chem. Rev.* **25**, 151–211, doi:10.1021/cr60081a002 (1939).
21. Jimenez-Lopez, C., Rodriguez-Navarro, A., Dominguez-Vera, J. M. & Garcia-Ruiz, J. M. Influence of lysozyme on the precipitation of calcium carbonate: A kinetic and morphologic study. *Geochim. Cosmochim. Acta* **67**, 1667–1676, doi:10.1016/s0016-7037(02)01275-9 (2003).

22. Ihli, J., Bots, P., Kulak, A., Benning, L. G. & Meldrum, F. C. Elucidating mechanisms of diffusion-based calcium carbonate synthesis leads to controlled mesocrystal formation. *Adv. Funct. Mater.* **23**, 1965–1973, doi:10.1002/adfm.201201742 (2013).
23. Yu, S. H. & Colfen, H. Bio-inspired crystal morphogenesis by hydrophilic polymers. *J. Mater. Chem.* **14**, 2124–2147, doi:10.1039/b401420k (2004).
24. Volkmer, D., Fricke, M., Huber, T. & Sewald, N. Acidic peptides acting as growth modifiers of calcite crystals. *Chem. Commun.*, 1872–1873, doi:10.1039/b405613b (2004).
25. Pokroy, B., Kapon, M., Marin, F., Adir, N. & Zolotoyabko, E. Protein-induced, previously unidentified twin form of calcite. *Proc. Natl. Acad. Sci. U. S. A.* **104**, 7337–7341, doi:10.1073/pnas.0608584104 (2007).
26. De Yoreo, J. J., Chung, S. & Friddle, R. W. In Situ atomic force microscopy as a tool for investigating interactions and assembly dynamics in biomolecular and biomineral systems. *Adv. Funct. Mater.* **23**, 2525–2538, doi:10.1002/adfm.201203424 (2013).
27. Friddle, R. W. *et al*. Single-molecule determination of the face-specific adsorption of amelogenin's C-Terminus on hydroxyapatite. *Angew. Chem., Int. Ed.* **50**, 7541–7545, doi:10.1002/anie.201100181 (2011).
28. Friddle, R. W., Noy, A. & De Yoreo, J. J. Interpreting the widespread nonlinear force spectra of intermolecular bonds. *Proc. Natl. Acad. Sci. U. S. A.* **109**, 13573–13578, doi:10.1073/pnas.1202946109 (2012).
29. Freeman, C. L., Harding, J. H., Quigley, D. & Rodger, P. M. Simulations of ovocleidin-17 binding to calcite surfaces and its implications for eggshell formation. *J. Phys. Chem. C* **115**, 8175–8183, doi:10.1021/jp200145m (2011).
30. Cooke, D. J., Gray, R. J., Sand, K. K., Stipp, S. L. S. & Elliott, J. A. Interaction of ethanol and water with the {10(1)over-bar4} surface of calcite. *Langmuir* **26**, 14520–14529, doi:10.1021/la100670k (2010).
31. Elhadj, S. *et al*. Peptide controls on calcite mineralization: Polyaspartate chain length affects growth kinetics and acts as a stereochemical switch on morphology. *Cryst. Growth Des.* **6**, 197–201, doi:10.1021/cg050288+ (2006).
32. Orme, C. A. *et al*. Formation of chiral morphologies through selective binding of amino acids to calcite surface steps. *Nature* **411**, 775–779, doi:10.1038/35081034 (2001).
33. Houk, K. N., Leach, A. G., Kim, S. P. & Zhang, X. Binding affinities of host-guest, protein-ligand, and protein-transition-state complexes. *Angew. Chem., Int. Ed.* **42**, 4872–4897, doi:10.1002/anie.200200565 (2003).

Acknowledgments

This material is based upon work supported as part of the Center for Nanoscale Control of Geologic CO_2, an Energy Frontier Research Center (EFRC), and performed as a user project at the Molecular Foundry, Lawrence Berkeley National Laboratory, both of which are funded by the U.S. Department of Energy, Office of Science, Office of Basic Energy Sciences under Contract No. DE-AC02-05CH11231. Pacific Northwest National Laboratory (PNNL) is multi-program national laboratory operated for Department of Energy by Battelle under Contracts No. DE-AC05-76RL01830. The authors thank Dr. Dongsheng Li for SEM data collection.

Author contributions

C.-L.C., R.Z. and J.J.D. conceived the study and wrote the manuscript. C.-L.C., J.Q. and J.T. performed experiments. C.-L.C., J.Q., J.T., R.Z. and J.J.D. analyzed the data.

Additional information

Supplementary information accompanies this paper at http://www.nature.com/scientificreports

Competing financial interests: The authors declare no competing financial interests.

How to cite this article: Chen, C.-L., Qi, J., Tao, J., Zuckermann, R.N. & DeYoreo, J.J. Tuning calcite morphology and growth acceleration by a rational design of highly stable protein-mimetics. *Sci. Rep.* **4**, 6266; DOI:10.1038/srep06266 (2014).